Single cell RNAseq provides a molecular and cellular cartography of changes to the human endometrium through the menstrual cycle

Wanxin Wang[1,7], Felipe Vilella[3,4,7], Inmaculada Moreno[3,4], Wenying Pan[1], Carlos Simon[3,4,5], and Stephen R. Quake[1,2,6]

[1]Department of Bioengineering,
[2]Department of Applied Physics,
[3]Department of Obstetrics & Gynecology,
Stanford University, Stanford, California, USA
[4]IGenomix Foundation, INCLIVA Health Research Institute, Valencia, Spain
[5]Department of Obstetrics & Gynecology, University of Valencia, Valencia, Spain
[6]Chan Zuckerberg Biohub, San Francisco, California, USA
[7]Equal contribution

Correspondence
carlos.simon@uv.es, quake@stanford.edu

Abstract
In a human menstrual cycle, the endometrium undergoes remodeling, shedding, and regeneration which are driven by substantial gene expression changes in the underlying cellular hierarchy. Despite its importance in human fertility and regenerative biology, mechanistic understanding of this unique type of tissue homeostasis remains rudimentary. Here, we characterized the transcriptomic transformation of human endometrium at single cell resolution, dissecting multidimensional cellular heterogeneity of the tissue across the entire natural menstrual cycle. We analyzed 6 endometrial cell types, including a previously uncharacterized ciliated epithelial cell type, during four major phases of endometrial transformation, and found characteristic signatures for each cell type and phase. We discovered that human window of implantation opens up with an abrupt and discontinuous transcriptomic activation in the epithelium, accompanied with widespread decidualized feature in the stroma. These data reveal signatures in the luminal and glandular epithelium during epithelial gland reconstruction, and suggest a mechanism for adult gland formation.

Introduction

The human menstrual cycle – with its monthly remodeling, shedding and regeneration of the endometrium – is not shared with many other species. Similar cycles have only been consistently observed in human, apes, and old world monkeys (*1*)(*2*) and not in any of the model organisms which undergo sexual reproduction such as mouse, zebrafish, or fly. This cyclic transformation is executed through dynamic changes in states and interactions of multiple cell types, including luminal and glandular epithelial cells, stromal cells, vascular endothelial cells, and infiltrating immune cells. Although different categorization schemes exist, the transformation can be primarily divided into two major stages by the event of

ovulation: the proliferative (pre-ovulatory) and secretory (post-ovulatory) stage (*3*). During the secretory stage, endometrium enters a narrow window of receptive state that is both structurally and biochemically ideal for embryo to implant (*4*)(*5*), i.e. the mid-secretory stage or the window of implantation (WOI). To prepare for this state, the tissue undergoes considerable reconstruction in the proliferative stage, during which one of the most essential elements is the formation of epithelial glands (*6*), lined by glandular epithelium.

Given the broad relevance in human fertility and regenerative biology, a systematic characterization of endometrial transformation across the natural menstrual cycle has been long pursued. Histological characterizations established the morphological definition of menstrual, proliferative, early-, mid-, and late- secretory stages (*3*). Bulk level transcriptomic profiling advanced the characterization to a molecular and quantitative level (*7*)(*8*), and demonstrated the feasibility of translating the definition into clinical diagnosis of the WOI (*9*). However, it has been a challenge to derive unbiased or mechanism-linked characterization from bulk-based readouts due to the uniquely heterogeneous and dynamic nature of endometrium.

The complexity of endometrium is unlike any other tissue: it consists of multiple cell types which vary dramatically in state through a monthly cycle as they enter and exit the cell cycle, remodel, and undergo various forms of differentiation with relatively rapid rates. The notable variance in menstrual cycle lengths within and between individuals (*10*) adds an additional variable to the system. Thus, transcriptomic characterization of endometrial transformation, at our current stage of understanding, requires that cell types and states be defined with minimum bias. High precision characterization and mechanistic understanding of hallmark events, such as the WOI, requires that we study both the static and dynamic aspects of the tissue. Single cell RNAseq provides an ideal platform for these purposes. We therefore performed a systematic transcriptomic delineation of human endometrium across the natural menstrual cycle at single cell resolution.

Results

To characterize endometrial transformation across the natural human menstrual cycle, we collected endometrial biopsies from 19 healthy and fertile females, 4-27 days after the onset of menstrual bleeding (**Figure S1**). All females were on regular menstrual cycles, with no influence from exogenous hormone or obstetrical pathology. Single cells were captured and cDNA was generated using Fluidigm C1 medium chips. Fraction of reads mapped to ERCC was used as the metric for quality filtering (Method).

Human endometrium consists of six cell types across the menstrual cycle

Dimensional reduction via t-distributed stochastic neighbor embedding (tSNE) (*11*) on top over-dispersed genes (Method) revealed clear segregation of cells into distinct groups (**Figure 1A**). We define cell types as segregations that are not time-associated, i.e. encompassing cells sampled across the menstrual cycle. Six cell types were thus identified; canonical markers and highly differentially expressed genes

enabled straightforward identification of four of these: stroma, endothelium, macrophage, and lymphocyte (**Figure 1B**). The two remaining cell types both expressed epithelium-associated markers; one of these cell types was characterized with an extensive list of uniquely expressed genes. Functional analysis revealed that 56% of genes in this list were annotated with a cilium-associated cellular component or biological process (**Figure 1C**, **Figure S2**), thereby identifying this cell type as "ciliated epithelium", specifically with motile cilia (*12*)(*13*). We defined the other epithelial cell type as "unciliated epithelium".

Endometrial transformation consists of four major phases across the menstrual cycle

Samples were taken throughout the menstrual cycle and annotated by the day of menstrual cycle (the number of days after the onset of last menstrual bleeding). While the time variable serves as an informative proxy for assigning endometrial states, it is susceptible to bias due to variances in menstrual cycle lengths between and within women (*10*), and limited in resolution due to variance of cells within an individual. To study transcriptomes of endometrial transformation in an unbiased manner, we performed within-cell type dimension reduction (tSNE) using whole transcriptome data from unciliated epithelium and stroma, respectively. The results revealed four major phases for both cell types, which we refer to as phase 1-4 (**Figure S3A**, **S3B**). The four phases were clearly time-associated (**Figure S3C**, **S3D**), confirming the overall validity of the time annotation. Examples where 1) the orders between two women in their phase assignments and time annotation were reversed, and 2) cells with the same time annotation were assigned into different phases, demonstrated the bias and imitated resolution if we were to use time directly for characterizations (**Figure S3**).

Constructing single cell resolution trajectories of menstrual cycle using mutual information based approach

Endometrial transformation over the menstrual cycle is at least in part a continuous process. A model that not only retains phase-wise characteristics but also allows delineation of continuous features between and within phases will enable higher precision characterizations. To build such a model, we used a mutual information (MI) (*14*) based approach, such that we exploited the information provided by the time annotation, minimized its limitation noted in the previous section, and accounted for potential continuity between and within phases. Briefly, we enriched for genes that were changing across the menstrual cycle based on the MI between gene expression and time annotation regardless of underlying model of dynamics (Method). In total we obtained 3,198 and 1,156 "time-associated" genes for unciliated epithelium and stroma, respectively (FDR<0.05) (**Figure S4A**). For both cell types, dimension reduction (tSNE) using time-associated genes revealed the same four major phases that we obtained using unsupervised approach (**Figure S4B**, **S4C**), demonstrating that the MI-based approach reduced the bias of the time annotation to the same extent as unsupervised approach. Meanwhile, the MI-based approach enabled identification of a clear trajectory that connected the phases and was time-associated within phases. We defined the trajectories using the principal

curve (*15*) (**Figure 2A**), and assigned each cell an order along the trajectory based on its projection on the curve, which we refer to as pseudotime (**Figure 2A**). We observed high correlations between time and pseudotime for both unciliated epithelium and stroma (**Figure 2B**). The high correlation between pseudotimes of the two cell types from the same woman (**Figure 2C**) further supported the validity of the trajectories.

The WOI opens with an abrupt and discontinuous transcriptomic activation in unciliated epithelium

Interestingly, we observed notable discontinuity in the trajectory of unciliated epithelium between phase 4 and the preceding phases (**Figure 2A**, left). This discontinuity was consistently observed regardless of the methods we used for dimension reduction (**Figure S5A**) or feature enrichment (**Figure S5B**). It was also unlikely to be due to low sampling density given that the involved biopsies were taken with a maximum interval of one day and that a similar discontinuity was not observed in the stroma counterpart (**Figure 2A**, right). To find the nature of this discontinuity, we explored the genes and their dynamics that contributed to it. Briefly, we identified genes that were dynamically changing along the single-cell trajectories of endometrial transformation by calculating the MI between gene expression and pseudotime, obtaining 1,382 and 527 genes for unciliated epithelial and stromal cells, respectively (FDR<1E-05, **Figure S6A**). Ordering these genes based on the pseudotime at which their global maximum was estimated to occur ($pseudotime_{max}$, Method) revealed the global features of transcriptomic dynamics across the menstrual cycle (**Figure S6B**). In unciliated epithelium, the dynamics demonstrated an overall continuous feature across phase 1-3, until an abrupt activation of a gene module marked the entrance into phase 4 (**Figure 3A**, **S6B**). Genes in this module included PAEP, GPX3, and CXCL14 (**Figure 3A**), among others which were relatively consistently reported by bulk transcriptomic profilings as overexpressed in WOI (*8*)(*16*). Thus, entrance into phase 4 can be identified with the opening of WOI. Our analysis revealed that this transition into the receptive state of the tissue occurs with an abrupt and discontinuous transcriptomic activation in unciliated epithelium.

The WOI is characterized with widespread decidualized feature in stroma

Unlike their epithelial counterparts, transcriptomic dynamics in stromal cells demonstrated more stage-wise characteristics, where genes were up-regulated in a modular form, revealing boundaries between phases (**Figure 3B**, **S6B**). In phase 4 stroma, the up-regulated gene module included DKK1, S100A4, and CRYAB, confirming the identity of WOI, although the transition was not as abrupt as in their epithelial counterparts (**Figure 3A**). In the same module, we noticed the decidualization initiating transcriptional factor FOXO1(*17*) and decidualized stromal marker IL15 (*18*). Importantly, while their upregulation in phase 4 was obvious, their expression was already noticeable in phase 3 in a lower percentage of cells and with lower expression level. Decidualization is the transformation of stromal cells commonly observed during pregnancy, where stromal cells transformed from elongated fibroblast-like cells into enlarged round cells with specific cytoskeleton

modifications, playing essential roles for embryo invasion and for pregnancy development (for review see *18*). Our data suggested that this process initiated before the opening of WOI in a small percentage of stromal cells, and that at the receptive state of tissue, decidualized features were widespread in stroma.

The WOI closes with continuous transcriptomic transitions

While the WOI opened up with an abrupt transcriptomic transition in unciliated epithelial cells, it closed with a more continuous transition dynamics (**Figure 3A**). Genes expressed in phase 4 unciliated epithelium were featured by three major groups with distinct dynamic characteristics. Group 1 genes (e.g. PAEP, GPX3) had sustained expression throughout the entire phase 4, and their expression remained noticeable until phase 1 of a new cycle. Group 2 genes (e.g. CXCL14, MAOA, DPP4, and the metallothioneins (MT1G, MT2A, MT1F, MT1X)), on the other hand, gradually decreased to zero towards the later part of phase 4, whereas group 3 genes (e.g. THBS1, MMP7) were upregulated at later part of the phase. These characteristics indicate a continuous and gradual transition from mid-secretory to late-secretory stage, thereby the closure of WOI.

The parallel transition in stromal cells was also characterized with similar three groups of genes (**Figure 3B**) and continuous dynamics. Specifically we observed a transition towards the later part of phase 4: gradual down-regulation of decidualization–associated genes (e.g. FOXO1 and IL15) and up-regulation of a separate module of genes (e.g. LMCD1, FGF7). These transitions revealed the final stage of decidualization at transcriptomic level, which, differing from that during pregnancy, ultimately leads to the shedding of the endometrium in a natural menstrual cycle.

Relationship between endometrial phases identified at transcriptome level and canonically defined endometrial stages

Since its formalization in 1950 (*3*), histological definition of endometrial stages, i.e. the proliferative, early-, mid-, and late-secretory stages, has been used as the gold standard in dating endometrial state. It usually serves as the ground truth in bulk-based profiling studies in categorizing endometrial states. Given that there were clear differences between our phase definition and the canonical definition, we investigated the relationship between the two.

Cell mitosis is one of the most distinct features for pre-ovulatory (proliferative) endometrium, hence the naming of proliferative stage. Thus, to identify the boundary between proliferative and secretory phases, we explored cell cycle activities across the menstrual cycle. Specifically, we defined endometrial cell cycle associated genes (**Figure S7A**, **S7B**, Method) and assigned cells into G1/S, G2/M, or non-cycling states. For both unciliated epithelial and stromal cells, cell cycling was observed in only a small fraction of cells across the menstrual cycle (**Figure S7C**, **S7D**). The fraction demonstrated phase-associated dynamics, where it was most elevated in phase 1, slightly decreased in phase 2, and almost completely ceased in later phases (**Figure S7C**, **S7D**, right). Therefore, phase 1 and 2 can be identified as

proliferative phases, and phase 3 and 4 as secretory phases. With the anchor provided by WOI, phase 3 can thus be identified with early secretory stage.

In phase 1, we observed sub-phases in both unciliated epithelial and stroma cells that are primarily characterized with genes that are gradually decreasing or increasing towards later part of the phases (**Figure 3A**, **B**, **S6B**). In unciliated epithelium, the gradually decreasing genes included phase 4 genes (e.g. PAEP, GPX3), as well as PLAU, which activates the degradation of blood plasma protein. The down-regulation of these genes suggested the end of menstrual bleeding, and hence the transition from menstrual to proliferative stage in the canonical definition. Phase 2 can therefore be identified as a second proliferate (late-proliferative) stage at transcriptome level, which was not described in canonical definition.

Thus, the alignment of our transcriptomically defined endometrial phases and trajectories with ground truth biological events (menstruation and ovulation) further supported the validity of our trajectories. In addition, transformation in proliferative endometrium was reported to be featured with gradual morphological changes and no distinct sub-stage features at histological level (*3*). Our phase definition revealed a transcriptomic level endometrial state (phase 2) that morphological characterizations did not capture.

Transcriptome signatures in deviating glandular and luminal epithelium supports a mechanism for adult epithelial gland formation

In unciliated epithelial cells, we noticed further segregation of cells (**Figure 4A**) in the direction perpendicular to the overall trajectory of the menstrual cycle. Independently performed dimension reduction (tSNE) on cells from each of the major phases (**Figure S8A**), excluding genes associated with cell cycles (**Figure S7A**, **S7B**), confirmed the observed segregations.

To identify the nature of the segregation, we performed differential expression analysis and found genes that consistently differentiated the subpopulations across multiple phases (**Figure 4B**). We examined immunohistochemistry staining of these genes in the Human Protein Atlas (*20*) and found that genes upregulated in one population stained intensely in epithelial glands, whereas genes upregulated in the other demonstrated no to low staining. Moreover, among these genes we found a few that were associated with luminal and glandular epithelium. ITGA1, which was reported to be consistently upregulated in glandular epithelium than in luminal epithelium, started to differentially express between the two populations at phase 2 and the differential expression persisted for the rest of cycle. WNT7A, reported to be exclusively expressed in luminal epithelium (*6*), was overexpressed in the other population in all proliferative phases (**Figure 4C**); SVIL, differentially expressed in the same population in all but phase 4, encodes supervillin, which was associated with microvilli structure responsible for plasma membrane transformation on luminal epithelium (*21*). Taking the above evidence together, the deviating subpopulations can be identified as the glandular and luminal epithelium.

Within the differentially expressed genes, we also noticed those that were previously reported to be critical for endometrial remodeling and embryo implantation (**Figure 4C**). They were characterized with unique dynamic features. For example, the metallothioneins (MT1E, MT1G, MT2A, MT1F) were unregulated in the luminal and glandular cells with a consistent lag in one phase. LIF, which was implicated in endometrial receptivity (*22*)(*23*)(*24*), was down-regulated in glandular epithelium throughout phase 2, 3, and early phase 4. MMP26, a metalloproteinase reported to be up-regulated in proliferative endometrium (*8*), was differentially expressed in glandular epithelium until phase 4. Of note, we observed no such differential expression in phase-defining genes presented in the earlier sections or housekeeping genes. (**Figure S8B**).

Compared to the consistent distinction between the ciliated and unciliated epithelium, the deviation between luminal and glandular epithelium at transcriptome level was much subtler and dynamic: it became noticeable at late phase 1 and was most pronounced in phase 2 (**Figure 4A** and **Figure S8A**). This observation was further supported the dynamics of differentially expressing genes such as HPGD, SULT1E1, LGR5, VTCN1, and ITGA1 (**Figure 4C**), among many others (**Figure S8C**), in that the maximum deviation of their expression in luminal and glandular cells was reached in phase 2 or the latest stage before ovulation.

Functional enrichment analysis (*25*)(*26*)(*27*) on genes overexpressed in luminal epithelium in phase 2 revealed extensive enrichments in morphogenesis and tubulogenesis at tissue level that lead to development of anatomic structures as well as morphogenesis at cell level that lead to differentiation (**Figure 4D**). In addition, the Wnt signaling pathway, associated with gland formation in early post-natal periods, was also enriched in this gene group, along with growth, ion transport, and angiogenesis. On the other hand, the most pronounced feature of the glandular subpopulation in the same phase was a consistently higher fraction of cycling cells compared to their luminal counterparts (**Figure S7C**, left). The co-occurrence of the ceasing cell cycle activity and maximized deviation between the two subpopulations in phase 2 also suggests that the important role proliferation plays in the process.

Thus, functional annotation of the signatures suggests that endometrial gland reconstruction in adult endometrium is executed through extensive morphogenesis and tube formation in luminal epithelium as well as proliferation activities that are locally concentrated at glandular epithelium, which, contrary to previous proposals (*28*)(*29*), is very similar to early post-natal gland formation (for review, see *29*).

Relative abundance of other endometrial cell types demonstrated phase-associated dynamics

Using the phase definition of unciliated epithelial and stromal cells, we assigned other endometrial cell types from the same woman into their respective phases, quantified their abundance across the cycle (**Figure S9**), and identified their phase-defining genes (**Figure S10**). We observed an overall increase in ciliated epithelial

cells across proliferative phases and a subsequent decrease in secretory phases. The rise in lymphocyte abundance from late-proliferative to secretory phases was notable (**Figure 5A**), whereas macrophages seemed to follow an opposite trend.

Decidualization in natural menstrual cycle was characterized with direct interplay between lymphocytes and stroma cells

Infiltrating lymphocytes were reported to play essential roles in decidualization during pregnancy, where they were primarily involved in decidual angiogenesis and regulating trophoblastic invasion (*31*). Their functions in decidualization during the natural menstrual cycle, however, remain to be defined. The dramatic increase in lymphocyte abundance in early secretory stage strongly suggested their involvement in decidualization (**Figure 5A**). We therefore characterized their transcriptomic dynamics across the menstrual cycle to explore their roles and their interactions with other endometrial cell types during decidualization.

Compared to their non-decidualized counterparts in secretory (phase 3) and proliferative phases, decidualized lymphocytes (phase 4) in natural menstrual cycle had increased expression of markers that are characteristic of uterine NK cells during pregnancy (CD69, ITGA1, NCAM1/CD56) (**Figure 5B**). They also expressed a more diverse repertoire of both activating and inhibitory NK receptors (NKR) responsible for recognizing major histocompatibility complex (MHC) class I molecules (**Figure 5B**). Lineage-wise, we observed lymphocytes expressing both NK and T cell markers and those expressing only NK markers (**Figure 5B**), and therefore classified them as CD3+ and CD3- NK cells. Particularly, for both CD3+ and CD3- NK cells, a noticeable rise in the fraction of cells expressing CD56, the canonical NK marker during pregnancy, occurred as early as the tissue transitioned from proliferative to secretory stage (**Figure S11**), suggesting that decidualization was initiated before the opening WOI.

We next identified genes that are dynamically changing in the NK cells across the menstrual cycle and characterized those that are associated with NK functionality (**Figure 5C**). In CD3- NK cells, we observed a significant rise in cytotoxic granule genes in decidualized endometrium (phase 4), with the exception of GNLY. In CD3+ NK cells, this rise in cytotoxic potential was manifested with an increase in CD8, while the elevation in cytotoxic granule genes was only moderate. For both CD3+ and CD3- cells, the increase in IL2 receptors expression was noticeable in phase 4. Equally notable were genes involved in IL2 elicited cell activation. As for the cytokine/chemokine repertoire, CD3- decidualized cells expressed high level of chemokines. Their CD3+ counterparts, although expressing a more diverse cytokine repertoire, demonstrated much lower chemokine expression. Lastly, both CD3+ and CD3- decidualized NK cells had elevated expression of genes associated with cell growth, but had negligible expression in angiogenesis associated genes (**Figure 5C**), in contrary to their counterparts during pregnancy.

Meanwhile, decidualized stromal cells upregulated immune-related genes that reciprocated those upregulated in phase 4 NK cells. With the diversification of NKR

observed in decidualized NK cells, we observed an overall elevation in MHC class I genes in decidualized stroma (**Figure 5D**), including HLA-A and HLA-B, which are recognized by activating NKR, as well as HLA-G, recognized by inhibitory NKR. With the IL2-elicited activation observed in decidualized NK cells, we noticed not only the elevation of IL15, which plays similar roles as IL2, as well as IL15 involved pathways that regulate lymphocyte activation and proliferation. Lastly, an angiogenesis associated pathway was elevated in decidualized stromal cells, complementing the lack of this functionality observed in decidualized NK cells.

Discussion

In this work, we studied both static and dynamic characteristics of the human endometrium across the menstrual cycle with single cell resolution. At the transcriptomic level, we used an unbiased approach to identify 6 major endometrial cell types, including a previously uncharacterized ciliated epithelial cell type, and four major phases of endometrial transformation. For the unciliated epithelial and stromal cells, we built high-resolution trajectories to track their remodeling through the menstrual cycle with minimum bias. Based on these fundamental units and structures, we identified and characterized the receptive state of the tissue with high precision, and studied the dynamic cellular and molecular transformations that lead to the state.

We discovered ciliated epithelium as a transcriptomically distinct endometrial cell type. They are consistently present but dynamically changing in abundance across the menstrual cycle (**Figure S9**). Thus, their molecular signatures and functions should be taken into account in future characterization of the tissue. We therefore provided the comprehensive transcriptomic signature with functional annotations for the cell type such that they can serve as molecular anchors for future studies. Particularly, we highlight the notably high fraction of genes (~25%) in this signature with no functional annotations (**Figure S2**). Co-expression of these genes with known cilium-associated genes and their exclusive activation in ciliated epithelium provides evidence for their cilium-associated functionality. In general, ciliary motility plays important roles in material transport and in signals sensing and transduction (*32*); its dysfunction can lead to both organ-specific diseases and multi-system syndromes (*32*)(*33*). Thus, functional studies that link the roles of these un-annotated genes with cilia functionality will also facilitate our understanding in this organelle in a broader picture.

We identified the opening of the WOI and discovered unique transcriptomic dynamics accompanying the transition. It was previously postulated that a continuous dynamics would better describes the entrance of WOI since human embryo implantation doesn't seem to be controlled by a single hormonal factor as in mice (*34*)(*35*), while discontinuous characteristics were also speculated based on morphological observation of plasma membrane transformation (*36*). Our data suggested that the WOI opens with an abrupt and discontinuous transcriptomic transition in unciliated epithelium, accompanied by a more continuous transition in stromal cells. Meanwhile, the abruptness of the transition also suggests that we

should be able to diagnose the opening of the WOI with high precision in clinical practices of embryo transfer.

The abrupt opening of the WOI also allowed us to elucidate the relationship between the WOI and decidualization. As noted earlier, decidualization is the transformation of stroma cells that is commonly observed during pregnancy in both human and mouse, supporting developments of implanted embryo. However, in contrary to mice where decidualization is triggered by implanting embryo(s)(*37*) and thus occurred exclusively during pregnancy, in human, decidualization occurs spontaneously during natural human menstrual cycles independent of the presence of a embryo (*22*). Thus, the relative timing between the WOI and the initiation of decidualization in human is unclear. Our data suggests that decidualization is initiated before the opening of the WOI, and that at the opening of the WOI, decidualized features were widespread in stromal cells.

We identified the transcriptomic signature in luminal and glandular epithelium during epithelial gland formation. The definition of luminal and glandular epithelium was established based on the distinct morphology and physical location between the two. Their distinction at transcriptome level had not been established. We found markers that differentiate the two across multiple phases of the menstrual cycle. Moreover, we discovered signatures that are differentially up-regulated in glandular and luminal epithelium during the formation of epithelial glands. Epithelial glands create proper biochemical milieu for embryo implantation and subsequent development of pregnancy. In human, the mechanism for their reconstruction during proliferative phases, however, is under debate. Our analysis suggests a mechanism that involves 1) extensive morphogenesis and tube formation and 2) cell differentiation in luminal epithelium, as well as proliferation activities that were locally concentrated at glandular epithelium. The mechanism suggests that glandular epithelium derives from luminal epithelium, in contrary to alternate proposals where it derives from stroma cells via mesenchymal to epithelial transition or cells from basal layer of the tissue (*28*)(*29*) (*30*).

Lastly, we provided evidence for the direct interplay between stroma and lymphocytes during decidualization in menstrual cycle. Our analysis suggested that, during decidualization in cycling endometrium, stromal cells are directly responsible for the activation of lymphocytes through IL2-eliciated pathways. Particularly interesting to us was the occurring diversification of activating and inhibitory NKR in NK cells and the overall up-regulation of MHC class I molecules in stromal cells. During pregnancy, cytotoxic NK cells were tolerant towards the semi-allogeneic fetus (*38*). This paradoxical phenomenon was hypothesized to be mediated by 1) the upregulation of non-classical MHC class I molecule (HLA-G) (*39*), the ligand to NK inhibitory receptor, and 2) the downregulation of classical MHC class I molecules (HLA-A, HLA-B) (*40*)(*41*) that engage with NK activating receptors. Our results demonstrate that similar suppression in NK cells with high cytotoxic potential occurs during natural menstrual cycle, however exerted by decidualized stromal cells.

Conclusion

In summary, we systematically characterized the human endometrium across the menstrual cycle from both static and dynamic perspective. The high resolution of the data and our analytical framework allowed us to answer previously unresolved questions that are centered on the tissue's receptivity. We envision that our findings and the comprehensive molecular signatures we present will provide theoretical foundations and molecular anchors for future studies. Our comprehensive dataset will also be a useful resource to answer questions and to device tools that go beyond those addressed in this study.

Material and method

Subject details

All procedures involving human endometrium were conducted in accordance with the Institutional Review Board guidelines for Stanford University and IVI/University of Valencia, including informed consent for tissue collection from all subjects. Tissue collection was approved by the IRB code 1603-IGX-016-CS of IVI Valencia, Spain. De-identified human endometrium was obtained from female aged 18-34, with regular menstrual cycle (3-4 days every 28-30 days), BMI ranging 19-29 kg/m^2 (inclusive), and negative serological tests for HIV, HBV, HCV, RPR and normal karyotype. Exclusion criteria were female with recent contraception (IUD in past 3 months; hormonal contraceptives in past 2 months), and pathological and/or medical conditions (uterine or adjuvant pathologies; bacterial, fungal, or viral infection).

Methods details

Endometrium tissue dissociation and population enrichment

A two-stage dissociation protocol was used to dissociate endometrium tissue and separate it into stroma and epithelium enriched single cell suspensions. Prior to the dissociation, the tissue was rinsed with DMEM (Sigma) on a petri dish to remove blood and mucus. Excess DMEM was removed after the rinsing. The tissue was then minced into pieces as small as possible, and dissociated in collagenase A1 (Sigma) overnight at 4 °C in a 50 mL falcon tube at horizontal position. This primary enzymatic step dissociates stroma into single cells while leaving epithelium glands and lumen mostly undigested. The resulting tissue suspension was then briefly homogenized and left un-agitated for 10 mins in a 50 mL Falcon tube at vertical position, during which epithelial glands and lumen sediment as a pellet and stromal cells stay suspended in the supernatant. The supernatant was therefore collected as the stroma-enriched suspension. The pellet was washed twice in 50 mL DMEM to further remove residual stroma cells. The washed pellet was then dissociated in 400 µL TrypLE Select (Life technology) for 20 mins at 37°C, during which homogenization was performed via intermittent pipetting. DNaseI (100 µL) was then added to the solution to digest extracellular genomic DNA. The digestion was quenched with 1.5 mL DMEM after 5 min incubation. The resulting cell suspension was then pipetted, filtered through a 50 µm cell strainer, and centrifuged at 1000 rpm for 5 min. The pellet was re-suspended as the epithelium-enriched suspension.

Single cell capture, imaging, and cDNA generation

For cell suspension of both portions, live cells were enriched via MACS dead cell removal kit (Miltenyi Biotec) following the manufacture's protocol. The resulting cell suspension was diluted in DMEM into a final concentration of 300-400 cells/μL before being loaded onto a medium C1 chip for mRNA Seq (Fluidigm). Live dead cell stain (Life Technology) was added directly into the cell suspension. Single cell capture, mRNA reverse-transcription, and cDNA amplification were performed on the Fluidigm C1 system using default scripts for mRNA Seq. All capture site images were recorded using an in-house built microscopic system at 20x magnification through phase, GFP, and Y3 channels. 1μL pre-diluted ERCC (Ambion) was added into the lysis mix, resulting in a final dilution factor of 1:80,000 in the mix.

Single cell RNAseq library generation

Single-cell cDNA concentration and size distribution were analyzed on a capillary electrophoresis-based automated fragment analyzer (Advanced Analytical). Tagmented and barcoded cDNA libraries were prepared only for cells imaged as singlet or empty at the captures site and with > 0.06 ng/uL cDNA generated. Library preparation was performed using Nextera XT DNA Sample Preparation kit (Illumina) on a Mosquito HTS liquid handler (TTP Labtech) following Fluidigm's single cell library preparation protocol with a 4x scale-down of all reagents. Dual-indexed single-cell libraries were pooled and sequenced in pair-end reads on Nextseq (Illumina) to a depth of 1-2 $\times 10^6$ reads per cell. bcl2fastq v2.17.1.14 was used to separate out the data for each single cell by using unique barcode combinations from the Nextera XT preparation and to generate *.fastq files.

Single cell RNAseq data analysis

Raw reads in the *.fastq files were trimmed to 75bp using fastqx, duplicate-removed using picard MarkDuplicates, and aligned to Ensembl human reference genome GRCh38.87 (dna.primary_assembly) using STAR (*42*) with default parameters. Aligned reads were converted to counts using HTSeq (*43*) and Ensembl GTF for GRCh38.87 under the setting -m intersection-strict \-s no. Downstream data analysis was performed in R. For each cell, counts were normalized to log transformed reads per million (log2(rpm)) by the equation $log_2(rpm) = log_2\left(1 + \frac{ct_{ij} * 1e06}{\sum ct_i}\right)$ where i is for cell i and j for gene j.

Quality filtering of single cells

For quality filtering, fraction of reads mapped to ERCC (f_{ERCC}) was used as the quality metric and empirical cumulative distribution of f_{ERCC} in empty capture sites recorded on the C1 chip was calculated and used as the null model ($ecdf_{null}$). Single cells retained for downstream analysis were those with ($ecdf_{null}(f_{ERCC})$) < 0.05. 2149 cells were retained for downstream analysis.

Differential expression analysis and functional enrichment

Differential gene-expression was performed using Wilcoxon's rank sum test.

Statistically significant differentially expressed genes were defined as those at least 2x fold overexpression and a rejected null hypothesis at a given FDR using Benjamini-Hochberg's procedure (*44*); P-values were adjusted using Yekutieli and Benjamini's method with monotonicity enforced (*45*). Functional enrichment analysis was performed using Gene Ontology Enrichement Analysis (http://www.geneontology.org).

Enrichment and identification of time-associated genes via mutual information

MI between gene expression and T or pseudot was calculated using the Java implementation of ARACNe-AP (*46*). FDR for the MI of each gene was estimated based on the empirical cumulative distribution between the expression of the gene and T or pseudot permutated with respect to cells. Smoothing of gene expression was performed with respect to pseudot using the R implementation of smooth spline (smooth.spline).

Cell heterogeneity analysis

Over-dispersion of genes was calculated as $\frac{CV_i^2}{CV_e^2}$, where CV_i^2 is the squared variation of coefficient of gene i across cells of interest and CV_e^2 is the expected squared variation of coefficient given mean, fitted using non-ERCC counts. All pairwise distances between cells were calculated as (1-Pearson's correlation). Dimensional reduction was performed using R implementation of tSNE (Rtsne).

Cell cycle analysis

We took a two-step approach in identifying cycling cells and defining endometrium-specific cell cycle signatures. We first used a published gene set encompassing 43 G1/S and 55 G2/M genes (*47*), representing the intersection of four previous gene sets (*48*)(*49*)(*50*), and calculated a G1/S and a G2/M score for all single cells in unciliated epithelial and stromal cells, respectively, following the scoring scheme in (*47*). Briefly, cells with at least 2x average expression of either G1/S or G2/M genes than the average of all cells in the respective cell type was assigned as putative cycling cells. We next performed Mann-Whitney U test (*51*) between the putative cycling cells and the rest of cells in the cell type to enrich for cell-cycle associated transcriptome signatures that were specific to endometrium (**Figure S2**). To assign cells into G1/S or G2/M stages, we performed dimension reduction on putative cycling cells using the identified signature, which revealed two major populations enriched in known G1/S or G2/M signatures. We assigned genes as either G1/S or G2/M associated by estimating the population at which peak expression of the gene occurred. We then recalculated the G1/S and G2/M scores for each cell using the signature customized for endometrium and finalized the assignment of G1/S and G2/M cells with at least 2x average G1/S or G2/M expression with respect to all cells in that cell type.

Data availability

The datasets generated and analyzed in the study are available in the NCBI Gene

Expression Omnibus (GEO) and Sequence Read Archive (SRA), and can be accessed upon request.

Acknowledgements
The authors would like to thank Hongxu Ding for valuable discussion and advice, Norma Neff and Jennifer Okamoto for sequencing expertise. This study was in jointly support by Howard Hughes Medical Institute, March of Dimes, Chan Zuckerburg Biohub, and MINECO/FEDER SAF-2015-67164-R(CS) (Spanish Government). WW was supported by the Stanford Bio-X Graduate Bowes Fellowship. FV was supported by Miguel Servet Program Type I of ISCIII [CP13/00038] and FIS project [PI14/00545].

Author Contributions
WW, WP, FV, CS, and SRQ conceived and designed the study. WW, FV, and IM performed experiments. WW performed single cell experiments. FV optimized the tissue dissociation protocol. IM performed tissue dissociation. WW and SRQ analyzed the data. WW, FV, CS, and SRQ interpreted the results. WW, FV, CS, and SRQ wrote the manuscript.

Competing interest
There is no conflict of interest.

References
1. R. D. Martin, The evolution of human reproduction: A primatological perspective. *Yearb. Phys. Anthropol.* **50** (2007), pp. 59–84.
2. D. Emera, R. Romero, G. Wagner, The evolution of menstruation: A new model for genetic assimilation: Explaining molecular origins of maternal responses to fetal invasiveness. *BioEssays*. **34**, 26–35 (2012).
3. R. W. Noyes, A. T. Hertig, J. Rock, Dating the Endometrial Biopsy. *Fertil. Steril.* **1**, 3–25 (1950).
4. H. B. Croxatto *et al.*, Studies on the duration of egg transport by the human oviduct. II. Ovum location at various intervals following luteinizing hormone peak. *Am. J. Obstet. Gynecol.* **132**, 629–634 (1978).
5. A. J. Wilcox, D. D. Baird, C. R. Weinberg, Time of Implantation of the Conceptus and Loss of Pregnancy. *N. Engl. J. Med.* **340**, 1796–1799 (1999).
6. J. Filant, T. E. Spencer, Uterine glands: Biological roles in conceptus implantation, uterine receptivity and decidualization. *Int. J. Dev. Biol.* **58** (2014), pp. 107–116.
7. A. Riesewijk *et al.*, Gene expression profiling of human endometrial receptivity on days LH+2 versus LH+7 by microarray technology. *Mol. Hum. Reprod.* **9**, 253–64 (2003).
8. M. Ruiz-Alonso, D. Blesa, C. Simón, The genomics of the human endometrium. *Biochim. Biophys. Acta - Mol. Basis Dis.* **1822**, 1931–1942 (2012).
9. P. Díaz-Gimeno *et al.*, A genomic diagnostic tool for human endometrial receptivity based on the transcriptomic signature. *Fertil. Steril.* **95**, 50–60 (2011).

10. Y. Guo, A. K. Manatunga, S. Chen, M. Marcus, Modeling menstrual cycle length using a mixture distribution. *Biostatistics*. **7**, 100–114 (2006).
11. L. Van Der Maaten, G. Hinton, Visualizing Data using t-SNE. *J. Mach. Learn. Res. 1*. **620**, 267–84 (2008).
12. F. Zhou, S. Roy, SnapShot: Motile Cilia. *Cell*. **162** (2015), p. 224–224.e1.
13. H. M. Mitchison, E. M. Valente, Motile and non-motile cilia in human pathology: from function to phenotypes. *J. Pathol.* **241** (2017), pp. 294–309.
14. G. Tkačik, A. M. Walczak, Information transmission in genetic regulatory networks: a review. *J. Phys. Condens. Matter*. **23**, 153102 (2011).
15. T. Hastie, W. Stuetzle, Principal curves. *J. Am. Stat. Assoc.* **84**, 502–516 (1989).
16. P. Díaz-Gimeno, M. Ruíz-Alonso, D. Blesa, C. Simón, Transcriptomics of the human endometrium. *Int. J. Dev. Biol.* **58**, 127–137 (2014).
17. Y. Park, M. C. Nnamani, J. Maziarz, G. P. Wagner, Cis-regulatory evolution of forkhead box O1 (FOXO1), a terminal selector gene for decidual stromal cell identity. *Mol. Biol. Evol.* **33**, 3161–3169 (2016).
18. H. Okada *et al.*, Regulation of decidualization and angiogenesis in the human endometrium: Mini review. *J. Obstet. Gynaecol. Res.* **40** (2014), pp. 1180–1187.
19. C. Y. Ramathal, I. C. Bagchi, R. N. Taylor, M. K. Bagchi, Endometrial decidualization: Of mice and men. *Semin. Reprod. Med.* **28** (2010), pp. 17–26.
20. M. Uhlen *et al.*, Tissue-based map of the human proteome. *Science (80-.).* **347**, 1260419–1260419 (2015).
21. S. Khurana, S. P. George, Regulation of cell structure and function by actin-binding proteins: Villin's perspective. *FEBS Lett.* **582** (2008), pp. 2128–2139.
22. J. Evans *et al.*, Fertile ground: Human endometrial programming and lessons in health and disease. *Nat. Rev. Endocrinol.* **12** (2016), pp. 654–667.
23. C. a White *et al.*, Blocking LIF action in the uterus by using a PEGylated antagonist prevents implantation: a nonhormonal contraceptive strategy. *Proc. Natl. Acad. Sci. U. S. A.* **104**, 19357–62 (2007).
24. J. Evans *et al.*, Prokineticin 1 mediates fetal-maternal dialogue regulating endometrial leukemia inhibitory factor. *FASEB J.* **23**, 2165–75 (2009).
25. M. Ashburner *et al.*, Gene ontology: Tool for the unification of biology. *Nat. Genet.* **25** (2000), pp. 25–29.
26. The Gene Ontology Consortium, Expansion of the Gene Ontology knowledgebase and resources. *Nucleic Acids Res.* **45**, D331–D338 (2017).
27. H. Mi *et al.*, PANTHER version 11: Expanded annotation data from Gene Ontology and Reactome pathways, and data analysis tool enhancements. *Nucleic Acids Res.* **45**, D183–D189 (2017).
28. O. W.C., A. C.I., S. R., Zonal changes in proliferation in the rhesus endometrium during the late secretory phase and menses. *Proc. Soc. Exp. Biol. Med.* **214** (1997), pp. 132–138.
29. C. C. Huang, G. D. Orvis, Y. Wang, R. R. Behringer, Stromal-to-epithelial transition during postpartum endometrial regeneration. *PLoS One*. **7** (2012), doi:10.1371/journal.pone.0044285.
30. P. S. Cooke, T. E. Spencer, F. F. Bartol, K. Hayashi, Uterine glands: Development, function and experimental model systems. *Mol. Hum. Reprod.* **19** (2013), pp. 547–558.

31. J. Hanna *et al.*, Decidual NK cells regulate key developmental processes at the human fetal-maternal interface. *Nat. Med.* **12**, 1065–1074 (2006).
32. B. W. Bisgrove, H. J. Yost, The roles of cilia in developmental disorders and disease. *Development*. **133**, 4131–4143 (2006).
33. M. Fliegauf, T. Benzing, H. Omran, When cilia go bad: Cilia defects and ciliopathies. *Nat. Rev. Mol. Cell Biol.* **8** (2007), pp. 880–893.
34. R. C. Hoversland, S. K. Dey, D. C. Johnson, Catechol estradiol induced implantation in the mouse. *Life Sci.* **30**, 1801–1804 (1982).
35. B. C. Paria, Y. M. Huet-Hudson, S. K. Dey, Blastocyst's state of activity determines the "window" of implantation in the receptive mouse uterus. *Proc. Natl. Acad. Sci. U. S. A.* **90**, 10159–62 (1993).
36. C. R. Murphy, Uterine receptivity and the plasma membrane transformation. *Cell Res.* **14** (2004), pp. 259–267.
37. J. Cha, X. Sun, S. K. Dey, Mechanisms of implantation: Strategies for successful pregnancy. *Nat. Med.* **18** (2012), pp. 1754–1767.
38. C. Schmitt, B. Ghazi, A. Bensussan, in *Reproductive BioMedicine Online* (2008), vol. 16, pp. 192–201.
39. R. Apps, L. Gardner, A. M. Sharkey, N. Holmes, A. Moffett, A homodimeric complex of HLA-G on normal trophoblast cells modulates antigen-presenting cells via LILRB1. *Eur. J. Immunol.* **37**, 1924–1937 (2007).
40. A. Moffett-King, Natural killer cells and pregnancy. *Nat. Rev. Immunol.* **2** (2002), pp. 656–663.
41. S. Sivori *et al.*, Triggering receptors involved in natural killer cell-mediated cytotoxicity against choriocarcinoma cell lines. *Hum. Immunol.* **61**, 1055–1058 (2000).
42. A. Dobin *et al.*, STAR: Ultrafast universal RNA-seq aligner. *Bioinformatics*. **29**, 15–21 (2013).
43. S. Anders, P. T. Pyl, W. Huber, HTSeq-A Python framework to work with high-throughput sequencing data. *Bioinformatics*. **31**, 166–169 (2015).
44. Y. Benjamini, Y. Hochberg, Controlling the false discovery rate: a practical and powerful approach to multiple testing. *J. R. Stat. Soc. B*. **57** (1995), pp. 289–300.
45. D. Yekutieli, Y. Benjamini, Resampling-based false discovery rate controlling multiple test procedures for correlated test statistics. *J. Stat. Plan. Inference*. **82**, 171–196 (1999).
46. A. Lachmann, F. M. Giorgi, G. Lopez, A. Califano, ARACNe-AP: Gene network reverse engineering through adaptive partitioning inference of mutual information. *Bioinformatics*. **32**, 2233–2235 (2016).
47. I. Tirosh *et al.*, Single-cell RNA-seq supports a developmental hierarchy in human oligodendroglioma. *Nature*. **539**, 309–313 (2016).
48. E. Z. Macosko *et al.*, Highly parallel genome-wide expression profiling of individual cells using nanoliter droplets. *Cell*. **161**, 1202–1214 (2015).
49. M. S. Kowalczyk *et al.*, Single-cell RNA-seq reveals changes in cell cycle and differentiation programs upon aging of hematopoietic stem cells. *Genome Res.* **25**, 1860–1872 (2015).
50. M. L. Whitfield, Identification of Genes Periodically Expressed in the Human

Cell Cycle and Their Expression in Tumors. *Mol. Biol. Cell*. **13**, 1977–2000 (2002).

51. H. B. Mann, D. R. Whitney, On a Test of Whether one of Two Random Variables is Stochastically Larger than the Other. *Ann. Math. Stat.* **18**, 50–60 (1947).

Figure captions

Figure 1. Definition of endometrial cell types at transcriptome level. A. Dimension reduction (tSNE) on all cells and top over-dispersed genes revealed six endometrial cell types. (top right inset: tSNE performed on immune cells only) **B.** Top discriminatory genes (differentially expressed genes expressed in > 85% cells in the given type) and canonical markers (red) for each identified cell type. **C.** Functional enrichment of uniquely expressed genes in ciliated epithelium. (FC: fold change)

Figure 2. Constructing trajectories of endometrial remodeling across the menstrual cycle at single cell resolution. A. Pseudotime assignment of unciliated epithelial (epi) and stromal (str) cells across the trajectory of menstrual cycle. (Trajectories: principal curves; numbers: major phases defined in **Fig. S3** and **S4**; start: start of a cycle) **B.** Correlation between pseudotime and time (the day of menstrual cycle). **C.** Correlation of pseudotime between epi and str from the same woman. (Dot: median of all cells from a woman; error bar: median absolute deviation)

Figure 3. Temporal transcriptome dynamics across the menstrual cycle. Exemplary phase and sub-phase defining genes, and relation between transcriptomically defined phases and canonical endometrial stages for **(A)** unciliated epithelial (epi) and **(B)** stromal (str) cells in **(C)** a human menstrual cycle. Cells in column were ordered by pseudotime. (Dashed line: continuous transition; WOI: window of implantation; pro: proliferative; sec: secretory)

Figure 4. Identification of subpopulations of unciliated epithelial cells across the trajectory of the menstrual cycle. A. Subpopulations of unciliated epithelial cells independently validated in **Fig. S8A** (gray: cells with ambiguous classification). Dynamics of genes **(B)** that differentially expressed between the two subpopulations across multiple phases, **(C)** that are previously reported to be implicated in endometrial remodeling or embryo implantation, and **(D)** that exemplified those that reached maximum differential expression in phase 2. (Dashed lines: X) **E.** Functional enrichment of genes overexpressed in luminal epithelium during epithelial gland formation. (Indented: terms belonging to the same GO hierarchy but with higher specificity as the term immediately above that had highest significance value)

Figure 5. Endometrial lymphocytes across the menstrual cycle and their interactions with other cell types during decidualization. A. Phase-associated abundance of endometrial lymphocytes normalized against stromal cells. **B.** Expression of markers identifying major lymphoid lineages. Cells (columns) were sorted based on percent expression of pan-markers for decidualized NK (NK) and NK cell receptors (NKR). **C.** Median expression of genes related to lymphocyte functionality. **D.** Functional annotation (left) and expression (right) of genes that were overexpressed in decidualized stroma (phase 4) that are implicated in immune responses.

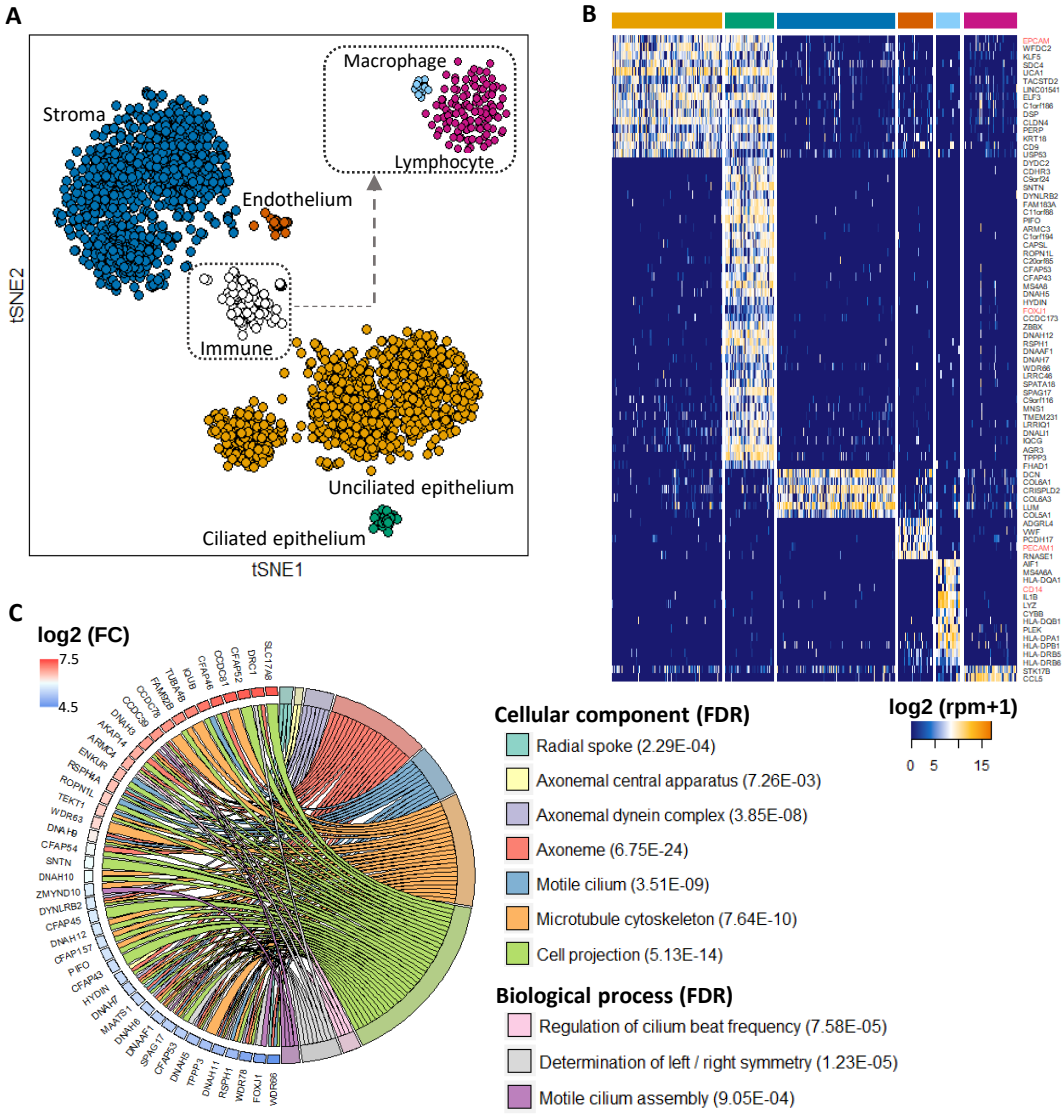

Figure 1. Definition of endometrial cell types at transcriptome level. A. Dimension reduction (tSNE) on all cells and top over-dispersed genes revealed six endometrial cell types. (top right inset: tSNE performed on immune cells only) **B.** Top discriminatory genes (differentially expressed genes expressed in > 85% cells in the given type) and canonical markers (red) for each identified cell type. **C.** Functional enrichment of uniquely expressed genes in ciliated epithelium. (FC: fold change)

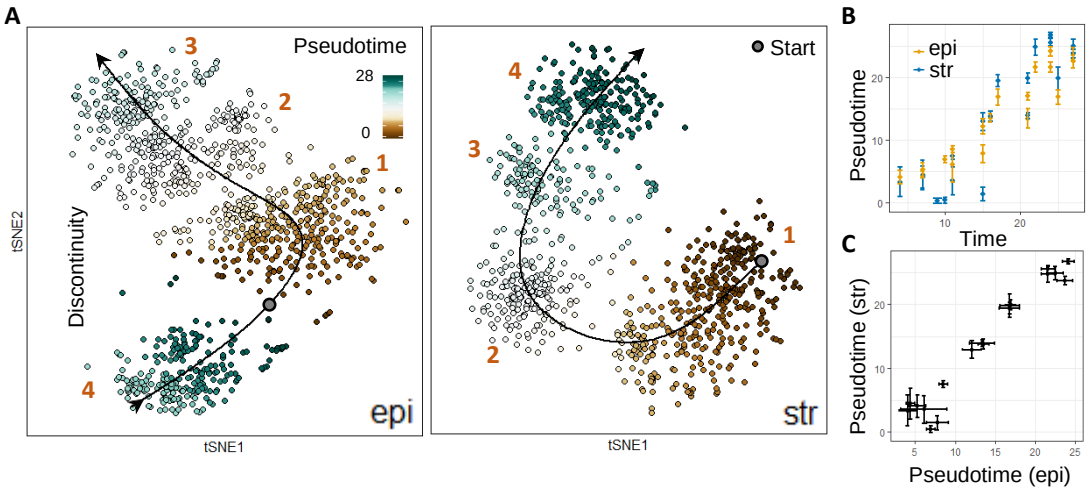

Figure 2. Constructing trajectories of endometrial remodeling across the menstrual cycle at single cell resolution. A. Pseudotime assignment of unciliated epithelial (epi) and stromal (str) cells across the trajectory of menstrual cycle. (Trajectories: principal curves; numbers: major phases defined in **Fig. S3** and **S4**; start: start of a cycle) **B.** Correlation between pseudotime and time (the day of menstrual cycle). **C.** Correlation of pseudotime between epi and str from the same woman. (Dot: median of all cells from a woman; error bar: median absolute deviation)

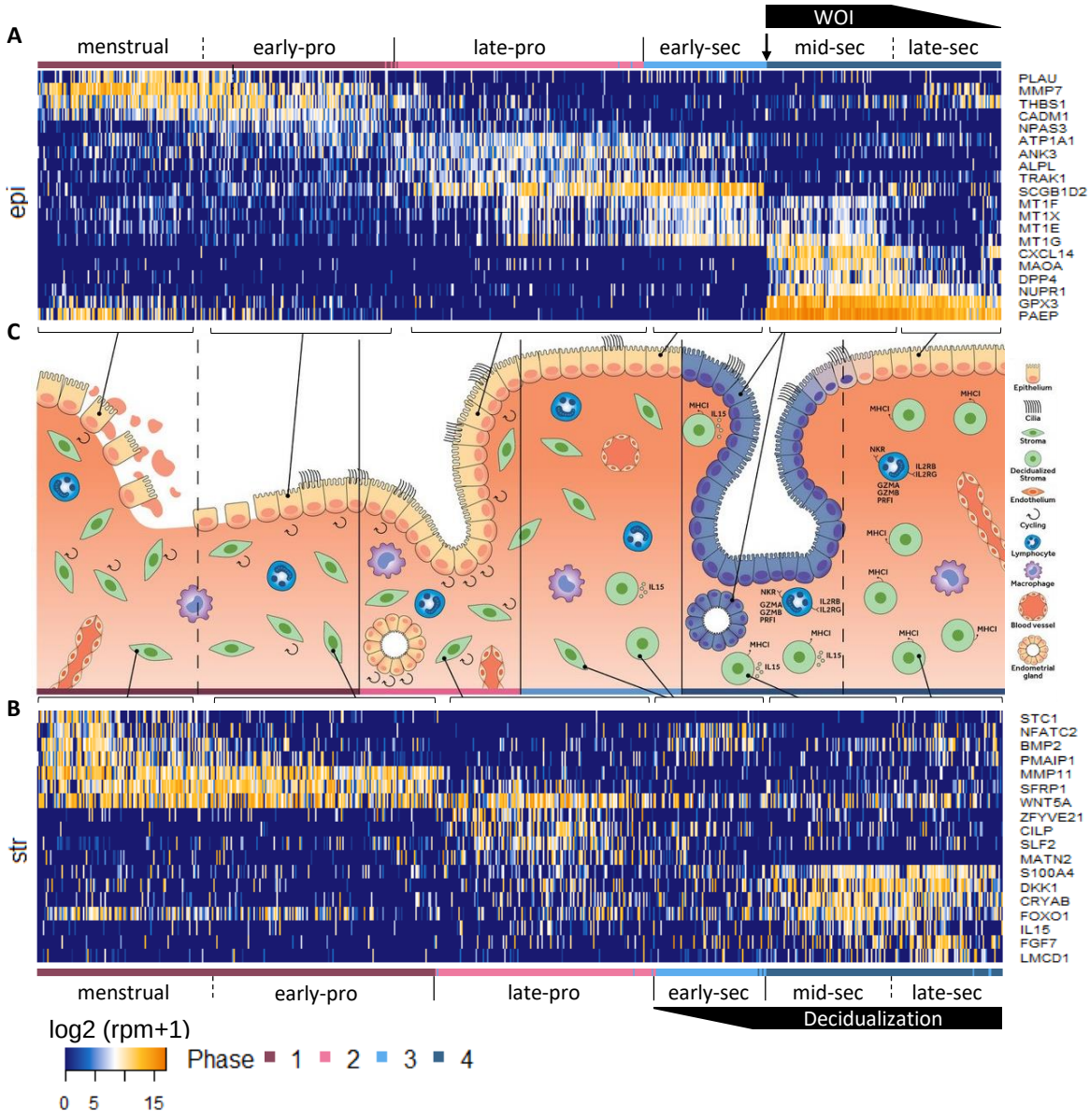

Figure 3. Temporal transcriptome dynamics across the menstrual cycle. Exemplary phase and sub-phase defining genes, and relation between transcriptomically defined phases and canonical endometrial stages for **(A)** unciliated epithelial (epi) and **(B)** stromal (str) cells in **(C)** a human menstrual cycle. Cells in column were ordered by pseudotime. (Dashed line: continuous transition; WOI: window of implantation; pro: proliferative; sec: secretory)

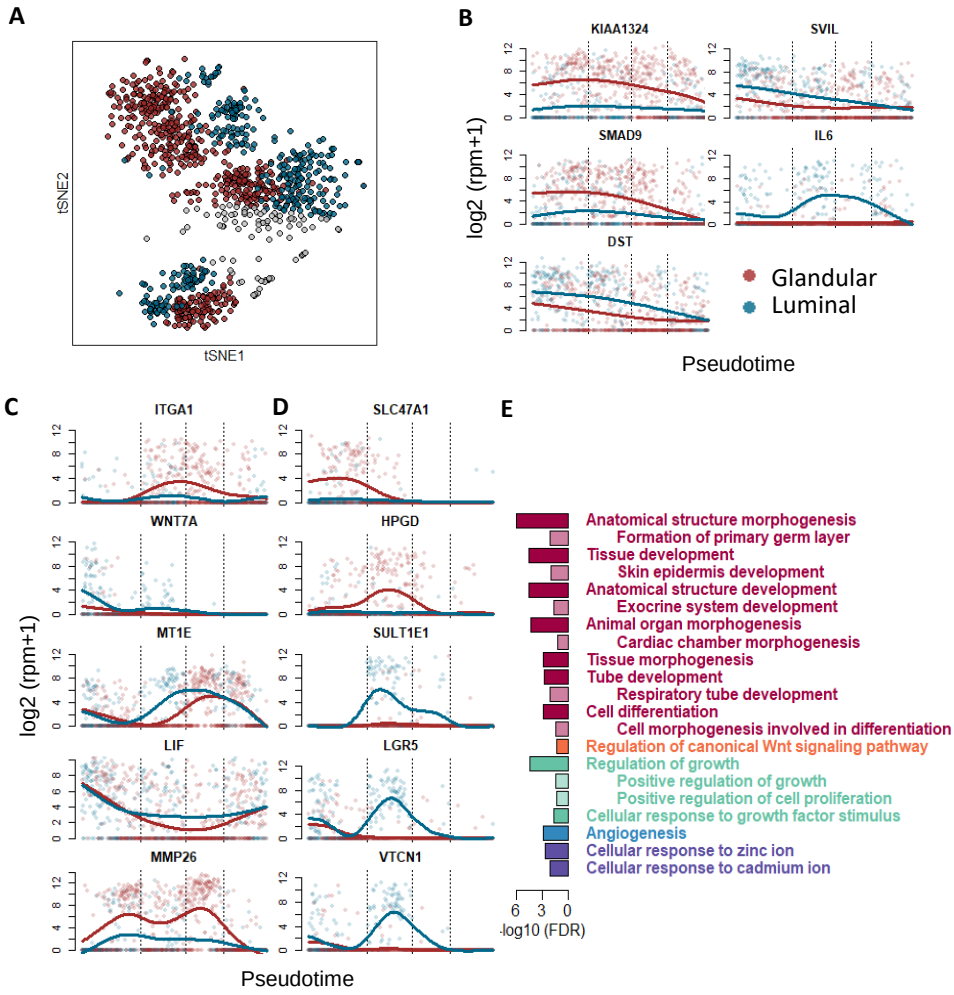

Figure 4. Identification of subpopulations of unciliated epithelial cells across the trajectory of the menstrual cycle. A. Subpopulations of unciliated epithelial cells independently validated in **Fig. S8A** (gray: cells with ambiguous classification). Dynamics of genes **(B)** that differentially expressed between the two subpopulations across multiple phases, **(C)** that are previously reported to be implicated in endometrial remodeling or embryo implantation, and **(D)** that exemplified those that reached maximum differential expression in phase 2. (Dashed lines: X) **E.** Functional enrichment of genes overexpressed in luminal epithelium during epithelial gland formation. (Indented: terms belonging to the same GO hierarchy but with higher specificity as the term immediately above that had highest significance value)

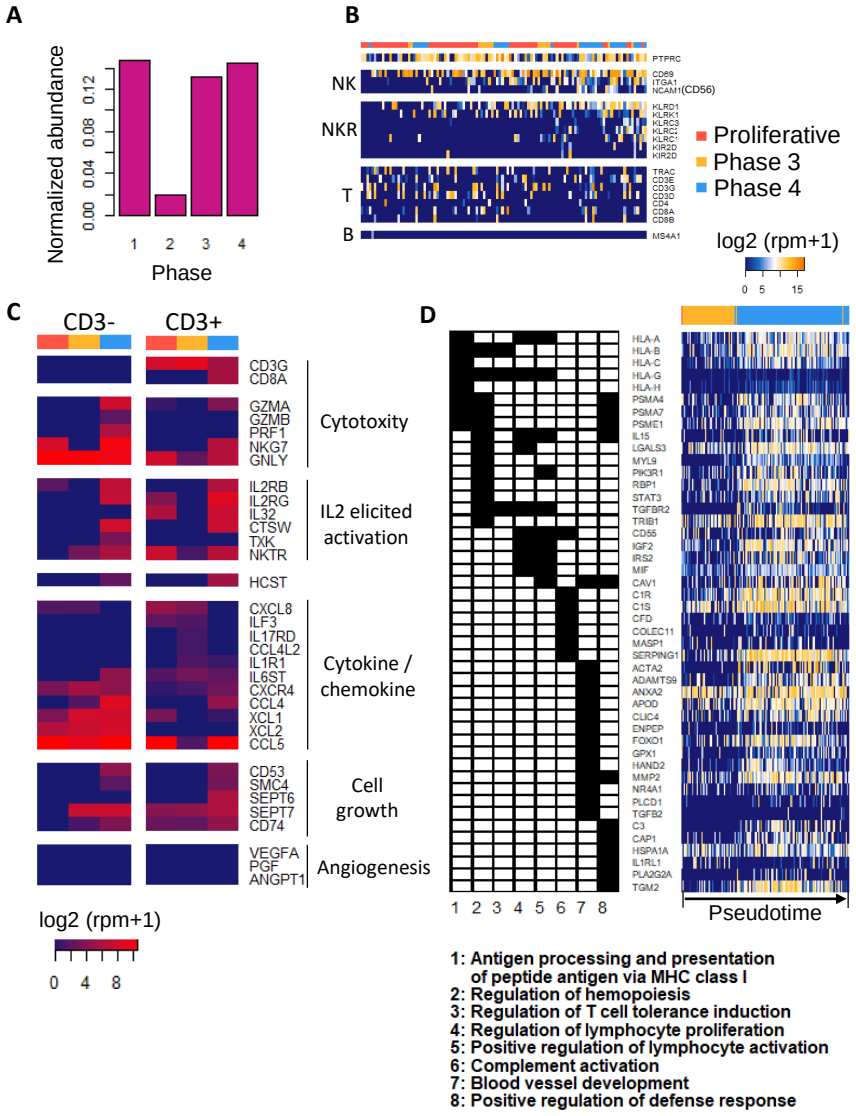

Figure 5. Endometrial lymphocytes across the menstrual cycle and their interactions with other cell types during decidualization. A. Phase-associated abundance of endometrial lymphocytes normalized against stromal cells. **B.** Expression of markers identifying major lymphoid lineages. Cells (columns) were sorted based on percent expression of pan-markers for decidualized NK (NK) and NK cell receptors (NKR). **C.** Median expression of genes related to lymphocyte functionality. **D.** Functional annotation (left) and expression (right) of genes that were overexpressed in decidualized stroma (phase 4) that are implicated in immune responses.